Plume Expansion and Ionization in a Micro Laser Plasma Thruster

Michael P. Reilly* and George H. Miley†
Department of Nuclear, Plasma, and Radiological Engineering, University of Illinois @ Urbana-Champaign, IL, 61801

William A. Hargus, Jr.‡
Air Force Research Laboratory, Edwards Air Force Base, CA. 93524

Ion density measurements have been performed on the plasma generated by an ablative diode laser thruster using a negatively biased flat plate probe. The biased probe data was coupled with measurement of the ablation crater through use of a scanning electron microscope (SEM). The SEM was used to analyze the post-pulse ablation spots to determine the volume of fuel ablated. The micro-laser plasma thruster (μLPT) discussed here ablates a target material through the back surface by focusing the laser through a transparent substrate in a process typically referred to as Transmissive mode (T-mode) ablation. The target materials investigated were polyvinyl chloride (PVC) and glycidyl azide polymer (GAP), while the substrates used were cellulose acetate and Kapton®. Peak ion densities for a GAP (target)/acetate (substrate) were found to be $1.6 \times 10^7 cm^{-3}$, while for GAP/kapton and PVC/acetate the peak ion densities were $4.5 \times 10^7 cm^{-3}$ and $7.9 \times 10^9 cm^{-3}$ respectively. Although these corresponded to low ionization fractions calculated from the observed mass loss, the results indicate there are ways to improve the ionization fraction and in turn increase the specific impulse.

Nomenclature

A_c	=	area of current flow [cm^2]
Δt	=	time step [s]
Δx	=	average length of fully developed plume [cm]
I_{sp}	=	specific impulse [s]
I	=	total ion current [A]
$\overline{n_{ion}}$	=	average ion density [cm^{-3}]
$\overline{N_{ion}}$	=	average number of ions per ablation shot [cm^{-3}]
$\overline{N_{fuel}}$	=	average number of particles per ablation shot [cm^{-3}]
q	=	charge [Coulombs]
v_{ion}	=	average ion velocity [cm/s]
f_{IONS}	=	ionization fraction
V_c	=	volume of charged particles [cm^3]
$n_{molecule}$	=	number of molecules per polymer
m_{fuel}	=	mass of fuel [g]

* Graduate Student, Nuclear, Plasma, and Radiological Engineering, 103 S. Goodwin MC-234, Urbana, IL. 61801, Student AIAA Member.
† Professor, Nuclear, Plasma, and Radiological Engineering, 103 S. Goodwin MC-234, Urbana, IL. 61801, Senior AIAA Member.
‡ Research Engineer, Air Force Research Laboratory, 10 E. Saturn Blvd, Edwards AFB, Senior AIAA Member.

Report Documentation Page

Form Approved
OMB No. 0704-0188

1. REPORT DATE	2. REPORT TYPE	3. DATES COVERED
JUN 2005		**-**

4. TITLE AND SUBTITLE	5a. CONTRACT NUMBER
Plume Expansion and Ionization in a Micro Laser Plasma Thruster (Paper)	5b. GRANT NUMBER
	5c. PROGRAM ELEMENT NUMBER
6. AUTHOR(S)	5d. PROJECT NUMBER
Michael Reilly; George Miley; William Hargus Jr.	**2308**
	5e. TASK NUMBER **0535**
	5f. WORK UNIT NUMBER
7. PERFORMING ORGANIZATION NAME(S) AND ADDRESS(ES)	8. PERFORMING ORGANIZATION REPORT NUMBER
Air Force Research Laboratory (AFMC),AFRL/PRSS,1 Ara Road,Edwards AFB,CA,93524-7013	
9. SPONSORING/MONITORING AGENCY NAME(S) AND ADDRESS(ES)	10. SPONSOR/MONITOR'S ACRONYM(S)
	11. SPONSOR/MONITOR'S REPORT NUMBER(S)

12. DISTRIBUTION/AVAILABILITY STATEMENT

Approved for public release; distribution unlimited

13. SUPPLEMENTARY NOTES

14. ABSTRACT

Ion density measurements have been performed on the plasma generated by an ablative diode laser thruster using a negatively biased flat plate probe. The biased probe data was coupled with measurement of the ablation crater through use of a scanning electron microscope (SEM). The SEM was used to analyze the post-pulse ablation spots to determine the volume of fuel ablated. The micro-laser plasma thruster (µLPT) discussed here ablates a target material through the back surface by focusing the laser through a transparent substrate in a process typically referred to as Transmissive mode (T-mode) ablation. The target materials investigated were polyvinyl chloride (PVC) and glycidyl azide polymer (GAP), while the substrates used were cellulose acetate and Kapton®. Peak ion densities for a GAP (target)/acetate (substrate) were found to be 1.6x10^7 cm-3, while for GAP/kapton and PVC/acetate the peak ion densities were 4.5x10^7 cm-3 and 7.9x10^9 cm-3 respectively. Although these corresponded to low ionization fractions calculated from the observed mass loss, the results indicate there are ways to improve the ionization fraction and in turn increase the specific impulse.

15. SUBJECT TERMS

16. SECURITY CLASSIFICATION OF:			17. LIMITATION OF ABSTRACT	18. NUMBER OF PAGES	19a. NAME OF RESPONSIBLE PERSON
a. REPORT	b. ABSTRACT	c. THIS PAGE			
unclassified	**unclassified**	**unclassified**		**13**	

ρ_{fuel} = density of fuel [g/cm^3]

V_{fuel} = volume of ablated fuel [cm^3]

r_{fuel} = radius of fuel ablation spot [cm]

d_{fuel} = depth of abated fuel spot [cm]

ϕ_c = diameter of discolored region on probe [cm]

MW_{fuel} = molecular weight of fuel [grams/mol]

N_A = Avogadro's number

I. Introduction

Lasers are becoming growingly critical in such applications as data storage, energy production through fusion, materials strengthening and fabrication, and communications. They are also increasingly vital as industrial companies researching extreme ultraviolet light for next generation lithography transition to a laser-based source. The understanding of laser-material interactions is of fundamental significance to enabling these technologies.

An additional application of lasers is that of a laser-based micro thruster for satellite propulsion[1]. Possible uses include primary propulsion of very small satellites as well as very precise attitude control for larger satellites. With the increasing availability and efficiencies of diode-based lasers, laser ablation of select materials provides a possible mechanism to produce micro electric thrusters[1]. The use of a micro Laser Plasma Thruster (μLPT) will allow for progress toward the development of nano- and pico- satellites, by allowing for an overall weight reduction due to the small size of this propulsion unit. An understanding of the ablation physics and plasma properties in the plume could lead to methods to achieve higher values of specific impulse (I_{sp}) and thrust.

There are two methodologies in which laser ablation produces useful thrust. In both cases, the plume of ablated material exhibits a $\cos^n(\theta)$ distribution with "n" varying between 5 and 20[2]. The first case is the reflective, or R-mode, illustrated in Figure 1, where the laser is incident on the front surface of the target mass. The laser heats the surface, boiling off material. This vapor phase material is then further heated by the incident flux. If the laser pulse is sufficiently intense, the heating produces a one dimensional planar expansion. This results in a nearly lossless thermal expansion. However, the R-mode is limited due to the coating of laser optics by the ablated materials. An alternative is to use the transmissive or T-mode geometry also illustrated in Figure 1. In this variation, the incident laser flux passes through a transmissive layer (substrate) to the ablatant.

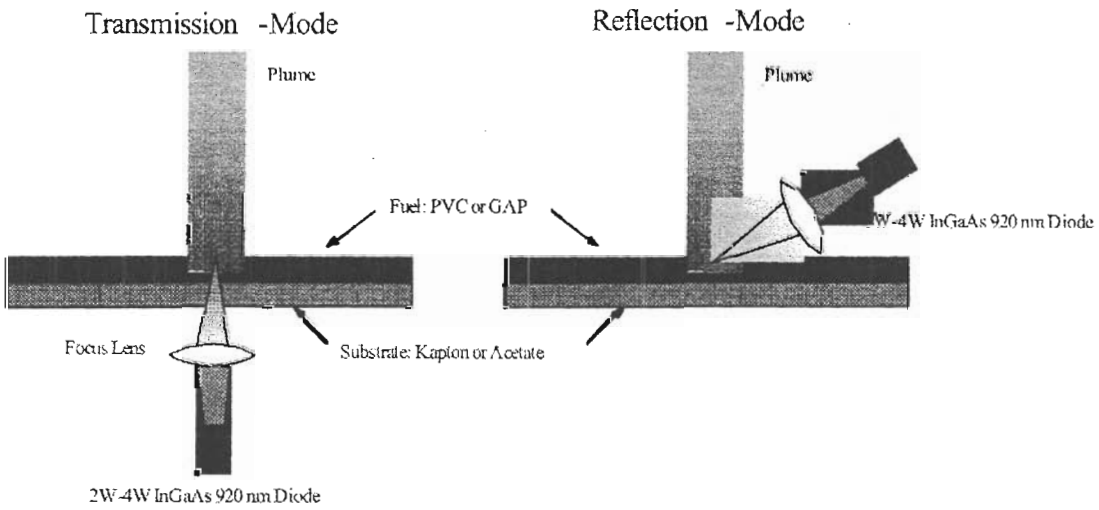

Figure 1. Transmissive Mode (T-mode) Ablation vs. Reflective Mode (R-mode) Ablation. *T-mode ablation protects the system optics but suffers from reduction in I_{sp} and exhaust momentum compared with R-mode. The R-mode, although enabling a greater I_{sp}, is lifetime restricted due to coating of optics by exhaust material.*

In the R-mode geometry a greater exhaust momentum and I_{sp} are achieved than the T-mode[2]. This is due to a layered ablation effect. In R-mode, the incident flux initially heats the outermost layer allowing for more laser energy to ionize the expanding material through absorption. A greater number of ionized particles will generate higher values of I_{sp}. In contrast to R-mode, the incident flux in T-mode, must heat all absorbing target material below the outermost layer before allowing the remaining energy to be directed toward ionizing the expanding material. This results in a lower exhaust momentum and lower I_{sp}. In fact, considering the extreme T-mode scenario where the target material is too thick; then all of the incident flux would be directed toward heating and possibly no ejection of material would occur.

In both modes, regardless of material thickness, it is favorable to keep the deposited energy near the laser focus spot. This reduces radial heating losses within the target. Therefore, materials with low thermal conductivities are considered especially for diode lasers with relatively low fluences. Specifically in this study, organic polymers are used as ablation targets in contrast to using metals. Not only does the low thermal conductivity of organic polymers reduce radial heating losses but it also relaxes the power requirement of the laser. However, the use of a low-voltage diode laser requires a longer pulse length to achieve the necessary fluence in order to initiate ablation. In this study, the laser fluence used is ~5kJ/cm^2.

II. Experimental Setup and Apparatus

Vacuum System

To accurately simulate the operational environment of space, a vacuum chamber was used to conduct tests on the μLPT's plume. Testing was conducted in a 50 cm diameter by 1 m long cylindrical vacuum chamber. The chamber is pumped by a Varian V-300 turbo-molecular vacuum pump with a pumping speed of 250 l/s backed by a dry scroll pump. Chamber pressure during testing is maintained in the 10^{-6} Torr range as measured with a Varian cold cathode ionization gauge. The vacuum chamber is mounted on 120x300x30 cm optics table. Both the table and turbo-molecular vacuum pump are vibration isolated. The optics table with pneumatic legs and the turbo-molecular vacuum pump with a vibration damping elastomer flange are shown in Figure 2.

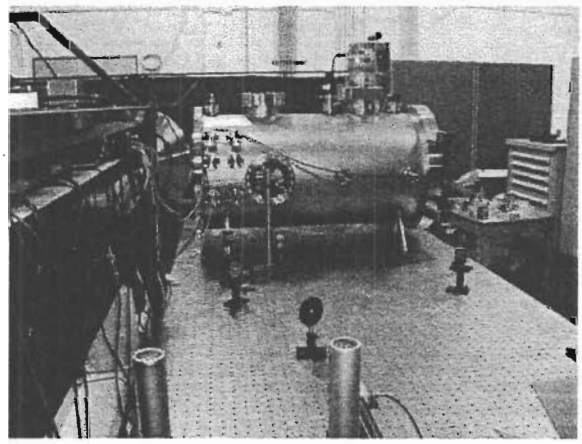

Figure 2. Vacuum system setup used in testing. *The chamber is seated on a 120x300x30 cm optics table with pneumatic legs.*

Single Shot μLPT

The μLPT apparatus used in these experiments employed a single shot prototype supplied to the Air Force Research Laboratory at Edwards AFB by Photonics Associates of Santa Fe, New Mexico. It utilizes a commercial 920 nano-meter wavelength, InGaAs low-voltage diode laser (JDS-UniPhase; Model SDL 6380-A). Although the laser power is low for ablation, (~4Watts), the tight focus of the beam yields high power densities (250kW/cm^2).

The single shot μLPT used in this study was specifically constructed for plume diagnostics. A flight model μLPT would have a mechanism to provide a greater propellant throughput. However, the essential physics

governing the ablation are identical. In the case of the single shot μLPT, the fuel is hard-mounted to the front of the device. Hard-mounted is defined to be that the fuel/substrate is secured to the front of the device with Kapton tape as shown in the schematic in Figure 3 and in the photograph shown in Figure 4. In this case, it is the aluminum mount with the fuel/substrate tape that is in motion. It is in this T-mode geometry where the laser is mounted behind the target/substrate material.

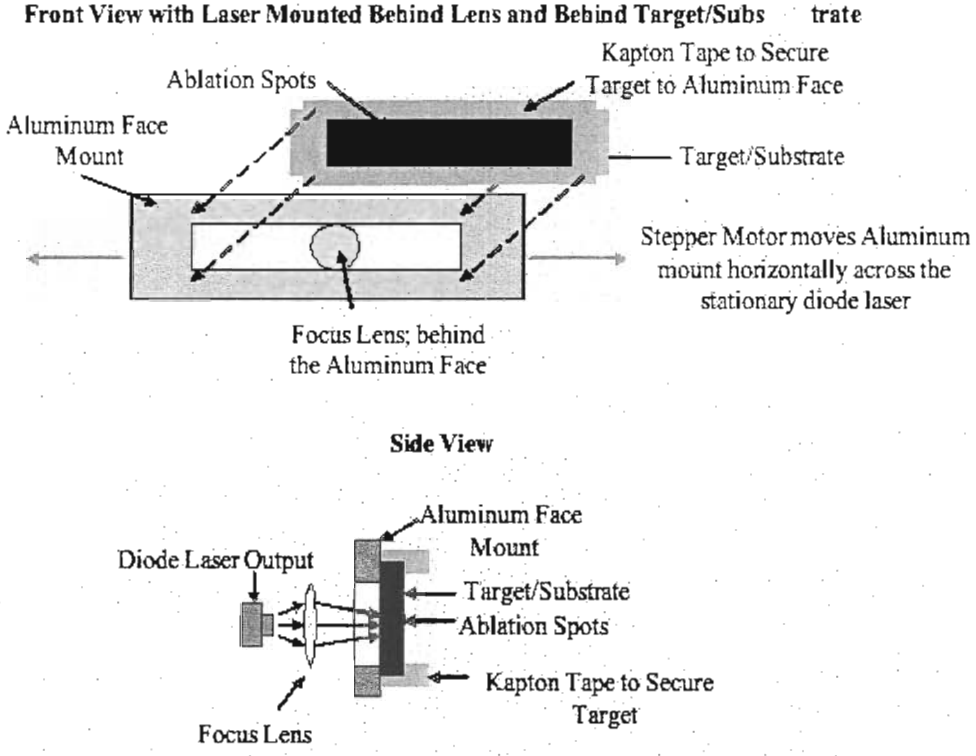

Figure 3. Mounting of Target/Substrate. *The fuel is secured to the mount with kapton tape around its edges. The stepper motor rasters the fuel in front of the focus lens and diode laser.*

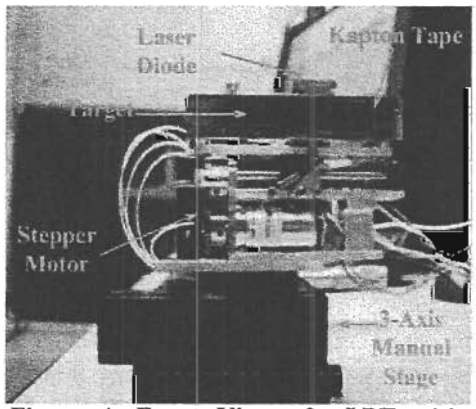

Figure 4. Front View of μLPT with Target/Substrate Mount. *The diode laser is transmitted from the rear of the target and particulate is ejected out of the page.*

The single shot μLPT shown in Figure 4 has precision control of each ablation shot so that a diagnostic can be performed on each ablation event. The movement of the target material is performed by a Labview program controlling a micro stepper motor (Figure 4) which horizontally traverses the target/substrate. This micro-stepper

uses an integral 76:1 step down gearbox acting through a 16:15 reduction gear. This allows for approximately 56400 steps for 5 cm of travel, corresponding to a control of about 1 μm. This control is ideal considering the μLPT's ablation spots are about 120±20 microns in diameter.

Figure 5 shows the μLPT in operation. This photograph of the plume was taken during the first half of the discharge. It visually measures about 4 cm in length. Pictures taken with a high speed camera show that on average the plume expands from the fuel face to this length during the first millisecond. Although this is typically what occurs, high speed photography showed that occasionally a smaller plume was evident. The variation in plume expansion during the first millisecond is shown in Figure 6.

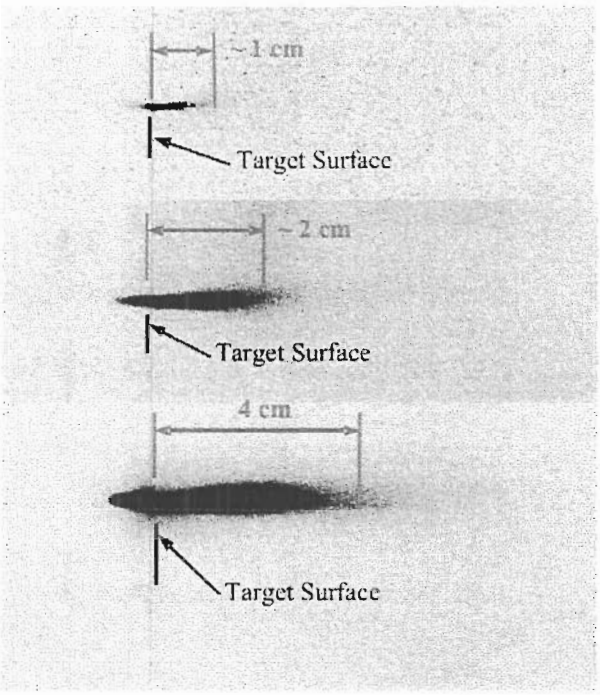

Figure 6. Plume Expansion from Target Surface. *All plumes are due to 24.5 mJ of deposited laser energy over 5 ms. Therefore, the topmost plume shows the smallest amount of ablated material being ejected. The average length of plume expansion during the first millisecond was observed to be 4 cm.*

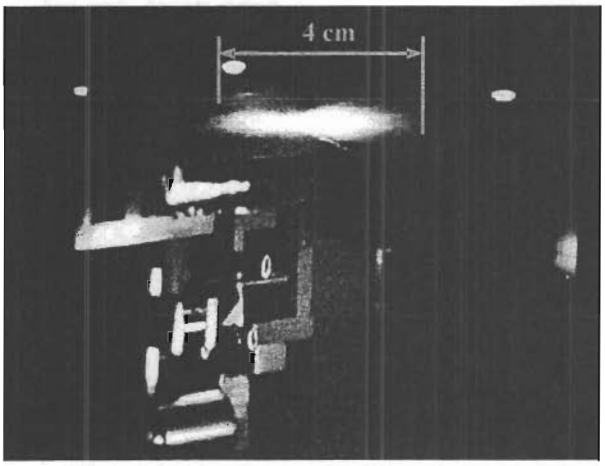

Figure 5. Photo of First 3 milliseconds of μLPT discharge. *Here the plume is visually estimated to be about 4 centimeters long.*

All three ablation events are the result of the same amount of laser energy being deposited; 24.5 mJ over 5 ms. These photographs do not indicate any relative degree of ionization between each event, however, the same amount of energy is deposited each time and therefore the difference in plume lengths is attributed to the thickness variations along the fuel surface. The plume expansion at the top of Figure 6 is due to a smaller amount of fuel being ablated than the other two expansions shown. As mentioned previously, the average length of the plume expansion during the first millisecond was observed to be 4 cm (bottom plume of Figure 6).

High speed photographs at later times of plume expansion were not observed because the setup required a second delayed trigger which was not employed at the time.

Ion Current Collection Probe

The negatively biased flat plate probe consists of a 15 cm diameter copper plate biased to -9V. The bias was performed using a dry cell battery. This bias technique is preferred to a DC power supply due the significant reduction in noise. It is assumed that the secondary electron emission from the low energy incident ions and neutrals is negligible[3]. Ion current measurements were performed by monitoring the voltage drop across a 200 kΩ resistor. A schematic of the probe is shown in Figure 7a and photograph in Figure 7b.

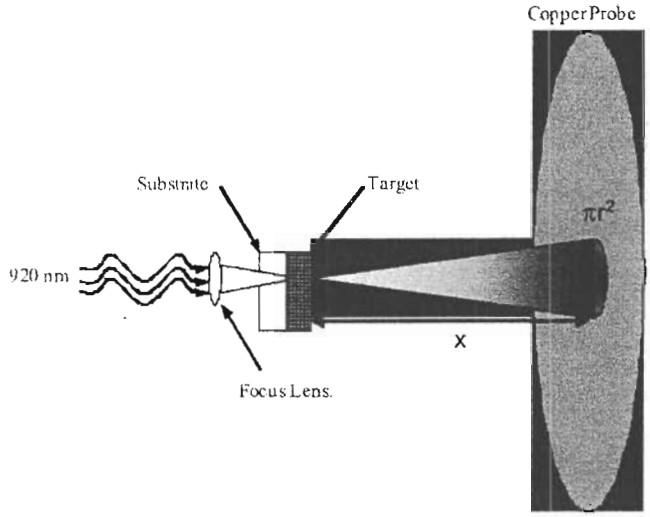

Figure 7a. μLPT T-mode with copper probe. *The copper probe was negatively biased with a 9V battery and ion currents were measured with secondary electron emission neglected.*

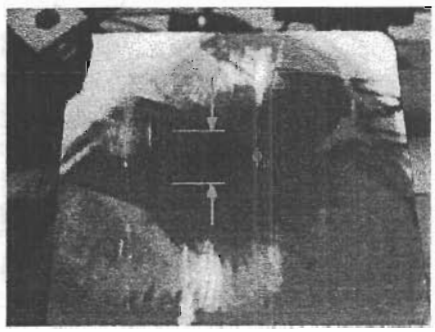

Figure 7b. Actual Probe used for ion current measurement. *The discoloration is due to 150 consecutive discharges at the same downstream location.*

There is a visible discoloration on the copper probe in Figure 7b due to the deposits of propellant particulates from a 150 shot series of μLPT firings. The arrows in Figure 7b denote the extent of the discoloration / deposits. It should be noted that in Figure 7b, some of the non-uniform appearance of the copper is due to its surface finish and is not the result of the incident plume. The diameter of the plume was taken from visual inspection of the width of the deposits on the probe. These were measured at each downstream location to determine the approximate diameter of the plume.

Target Material and Substrate

The combinations of target/substrate considered were a 60 micron thick fuel strip of Polyvinyl Chloride (PVC) layered on top of a 100 micron thick substrate of cellulose acetate and a 300 micron thick fuel strip of Glycidyl Azide Polymer (GAP) layered on top of a 60 micron thick substrate of cellulose acetate or kapton. The target/substrate thickness was determined from scanning electron microscope (SEM) measurement. Some of the physical characteristics[4-6] for these materials are listed in Table 1.

Table 1. Physical Characteristics of Target Materials and Substrates.

Target	Chemical Formula	Density
Glycidyl Azide Polymer	$C_3H_5ON_3$	1.29 g/cm^3
Polyvinyl Chloride	CH_2CHCl	1.35 g/cm^3
Substrate	**Index of Refraction**	**Density**
Acetate	1.48	1.22 g/cm^3
Kapton	1.70	1.42 g/cm^3

Note: the indices of refraction listed for the substrate materials are those for the sodium D-line at 589.3 nm.

III. Calculations

Average Ion Density

Taking an average over the target-to-probe distance and over the discharge time, the average ion density $\bar{n}_{ion}$ in the plume can be obtained through a measurement of the probe current using the relation[7]:

$$I = \bar{n}_{ion} q v_{ion} A_c \;;\; \bar{n}_{ion} = \frac{I}{q v_{ion} A_c} \tag{1}$$

In this expression, I is the total current collected on the biased probe and singly ionized plasma was assumed, so $q=1$. To ensure that the total current was measured, the probe was made much larger than the plume. The area of current flow, A_c, was approximated from the probe discoloration discussed earlier relative to Figure 7b. The ion velocity, v_{ion}, can be written as:

$$v_{ion} = \frac{dx}{dt} \cong \frac{\Delta x}{I \Delta t} \tag{2}$$

where Δx is the distance from the target face to the probe and Δt is the time step such that $I\Delta t$ is the total charge collected by the probe. The average ion density can then be calculated by assuming an average ion velocity over the five millisecond discharge of the μLPT. Then substituting (2) into (1), the averaged ion density becomes:

$$\bar{n}_{ion} = \frac{I \Delta t}{A_c \Delta x} \tag{3}$$

Then taking V_c as the volume of charged particles found from approximating the plume as a cone with the base ϕ_c determined by the discoloration of repetitively firing the device at the probe as shown in Figure 7b

$$V_c = A_c \Delta x \tag{4}$$

where ϕ_c and Δx were also used to calculated the plume angle of expansion illustrated in Figure 8

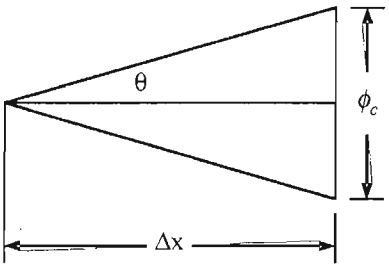

$$\theta = \tan^{-1}\left(\frac{\phi_c}{2\Delta x}\right) \tag{5}$$

Figure 8. Plume expansion depiction.

Typically, the half angle of the plume expansion is approximately 19°. Finally, with the total charge collected and the volume calculated, substituting (4) into (3) gives an expression for the average ion density as:

$$\bar{n}_{ion} = \frac{I \Delta t}{V_c} \tag{6}$$

This relation is the result of averaging over the discharge time as well as averaging over the spatial distance from the fuel surface to the probe.

Ionization Fraction

In addition to calculating the average ion density of plume, the ionization fraction can be approximately calculated using the average number of particles ejected per shot with the average ion density measurement:

$$f_{IONS} = \frac{\bar{N}_{ion}}{\bar{N}_{fuel}} \tag{7}$$

where the bar indicates an average over time and space. The average number of ions per ablation shot was taken as:

$$\overline{N}_{ion} = \overline{n}_{ion} V_{fuel} \tag{8}$$

V_{fuel} here is different than V_c, the volume of charged particles in the plume. V_{fuel} is the volume of the ablated fuel illustrated in Figure 9a with a corresponding SEM photo shown in Figure 9b. The area of the fuel A_{fuel} and the depth of the fuel d_{fuel} are taken from the SEM photo of Figure 7b.

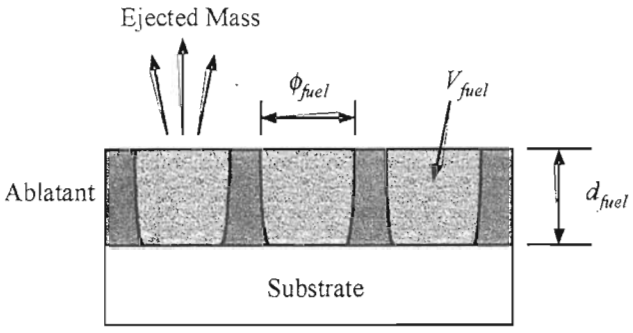

Figure 9a. Ionization fraction calculation. *The cross-hatched section is the volume of the fuel ablated.*

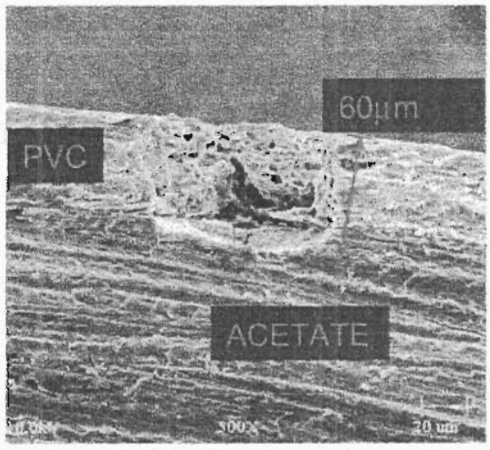

Figure 9b. SEM photo of PVC/Acetate Ablation Spot. *The SEM shows a nearly cylindrical ablation crater with a slight burning of the substrate.*

Utilizing the following definitions,

$$A_{fuel} = \pi r_{fuel}^2 \tag{9}$$

$$V_{fuel} = A_{fuel} d_{fuel} \tag{10}$$

$$m_{fuel} = V_{fuel} \rho_{fuel} \tag{11}$$

the number of total particles per ablation shot was calculated from:

$$\overline{N}_{fuel} = \frac{m_{fuel} N_A}{MW_{fuel}} n_{molecule} \tag{12}$$

In this expression, the total number of particles per ablation shot is defined as:

$$\overline{N_{fuel}} = \frac{(mass\ loss\ in\ grams)(\#\ molecules\ per\ mol)}{(grams\ per\ mol)}\ (particles\ per\ molecule) \tag{13}$$

here, $n_{molecule}$ is the number of per molecule in PVC or GAP. This value is necessary to calculate the ionization fraction f_{ions} or the total number of ions created to the total number of atoms ejected.

IV. Results

GAP/Acetate

The first target/substrate that will be discussed is the GAP/Acetate. Scanning Electron Microscope (SEM) analysis (Figure 10a-10b) shows that the ablation spot diameter on the GAP is 130±10μm. These spot sizes are for when the laser deposited 24.5 mJ over 5 ms. The depth of the ablation spots is 300μm, which is the full thickness of the GAP as shown in Figure 10a-10b. The substrate thickness is 60μm and there is little to no visible burning of the substrate by laser ablation when viewing SEM results. However, regarding the different substrates, there is expected to be some attenuation loss in laser energy due to their different indices of refraction[8] (Table 1).

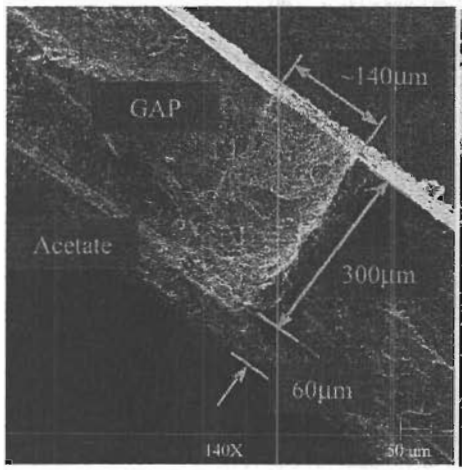

Figure 10a. GAP/Acetate SEM photo. *The target/substrate thickness and depth of ablation crater are visible.*

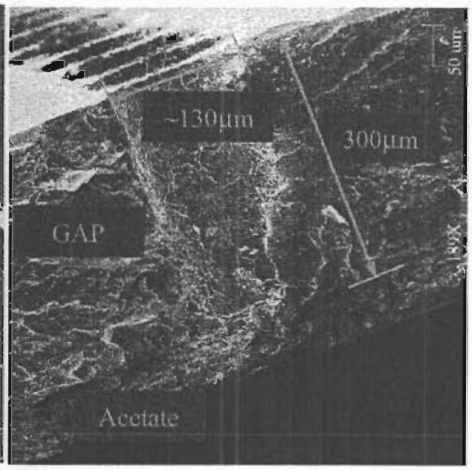

Figure 10b. GAP/Acetate SEM photo. *This is a different ablation crater than Figure 10a but similar results are observed.*

The average volume of the GAP ablated measured from SEM results was $4.0 \times 10^{-6} cm^3$. This corresponded to an average of 5.1×10^{-6}g/shot or 5.1μg/shot of ejected GAP. This calculation was simply based on the material density of the GAP from Table 1.

The average ion current profiles for 150 successive shots on the same fuel strip over the 5 ms discharge are shown in Figure 11. Error bars were determined as the standard deviation of 150 individual current profiles. The dip at the start of the discharge and the spike at the end of the discharge is electrical noise from the laser switching on/off. Each of the three profiles seen here are the result of averaging over 150 sequentially pulsed discharges on the same fuel strip. The figure indicates that using two different fuel strips of GAP/Acetate, similar performance is reached. This is evident in the similar magnitudes in the peak ion currents between fuel strip 1 and fuel strip 2. The peak currents are between 130-160 nano-Amps.

Interest was given to the downstream location where ion current reach a maximum. This location was found to be about 7 cm downstream of the target face. The average ion density 7 cm from the target face was $1.6 \times 10^{7} cm^{-3}$. This corresponded to an ionization fraction of 9.8×10^{-9} found from the ratio of the number of ions to the total number of particles ejected (Equation 7).

The variation in peak ion currents across each fuel strip is shown in Figure 12. The distance that these 150 ablation shots cover on the fuel strip is 2.5 cm. Over this distance the peak ion current experiences highs and lows which are assumed to be due to local fuel thickness variations.

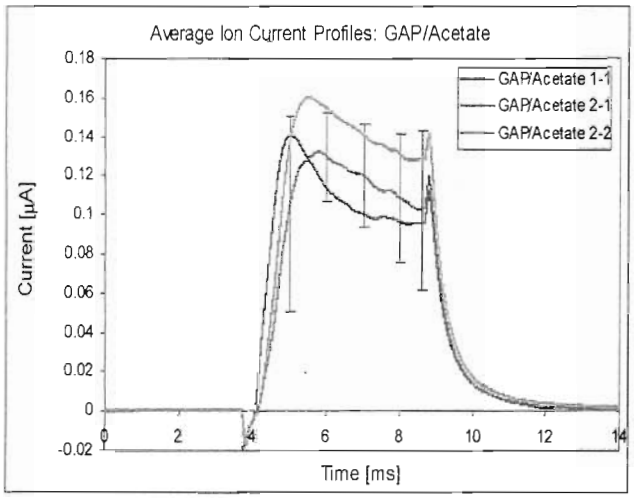

Figure 11. GAP/Acetate average ion currents. *The traces are for 24.5mJ deposited over 5ms. GAP/Acetate 1-1 represents one sample taken from fuel strip #1, whereas 2-1 and 2-2 indicate samples 1 and two taken from a separate fuel strip.*

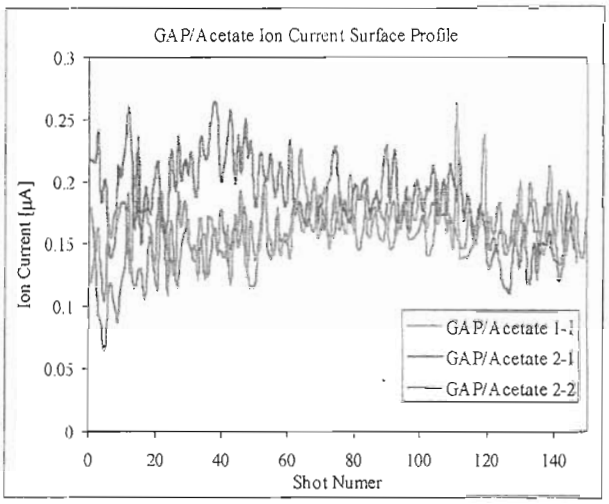

Figure 12. GAP/Acetate average ion currents. *The traces are for 24.5mJ deposited over 5ms. Traces were taken at 150 successive fuel locations. GAP/Acetate 1-1 represents one sample taken from fuel strip #1, whereas 2-1 and 2-2 indicate samples 1 and two taken from a separate fuel strip.*

GAP/Kapton

The same target material GAP is again studied, but with a Kapton substrate in contrast to acetate. SEM analysis shows the fuel thickness of the GAP is 100μm while the kapton is 160μm thick (Figure 13). The fuel thickness of the GAP/Kapton is not as thick as the previous GAP/Acetate (300μm GAP/Acetate versus 100μm GAP/Kapton; Figure 10a-10b). The ablation crater diameters again are 130±10μm as shown in Figure 13. These are similar to the GAP/Acetate case, although now because of the difference in thickness of the GAP, the average volume of mass ablated is $1.3 \times 10^{-6} cm^3$. This total volume of mass ablated is lower than when the GAP was backed with acetate. The amount of GAP mass ejected is calculated to be 1.7μg/shot, a 33% reduction when compared with GAP/Acetate.

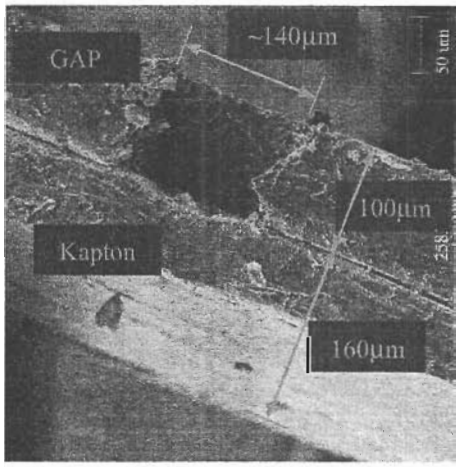

Figure 13. GAP/Kapton SEM photo. *The target/substrate and depth of ablation crater are visible here.*

The average ion current profiles are shown in Figure 14. The peak ion currents are between 600nA and 1μA. This is significantly higher than when the GAP was backed with acetate. However, this result should be expected. In this case, the GAP thickness was reduced by a factor of three and less total mass was ejected, but approximately the same amount of laser energy was deposited. With more laser energy now available for ionization instead of heating and neutral particle ejection, a higher ionization level is expected.

The downstream location where the ion current peaks is again 7 cm from the target face. The average ion density measured here is $4.5 \times 10^{7} cm^{-3}$ while the calculated average ionization fraction is 8.2×10^{-8}. Although the downstream location of the peak ion currents is the same for both GAP cases, the greater peak ion currents are again consistent with the smaller thickness GAP backed with Kapton.

The peak ion currents were again measured over 150 shots across 2.5 cm of the fuel. This result is illustrated in Figure 15. The peak values of the average ion currents for the Kapton backed GAP are shown to be significantly higher than when the GAP is backed with acetate. This is again attributed to the thickness of the target material. When there is less material, more of the laser energy can be transmitted through the substrate and subsequently directed toward ionization, as evident with the higher ion density and ionization fraction for the Kapton backed as opposed to the Acetate backed GAP. The resulting lower ion densities and ionization fractions from the

GAP/Acetate are due to more of the deposited laser energy going into heating the thicker material as opposed to ionizing the thinner GAP/Kapton.

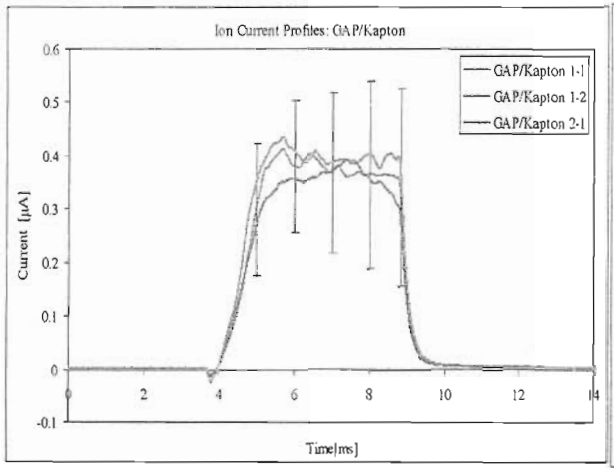

Figure 14. GAP/Kapton average ion currents. *The traces are for 24.5mJ deposited over 5ms. GAP/Kapton 1-1 represents one sample taken from fuel strip #1, whereas 2-1 and 2-2 indicate samples 1 and two taken from a separate fuel strip.*

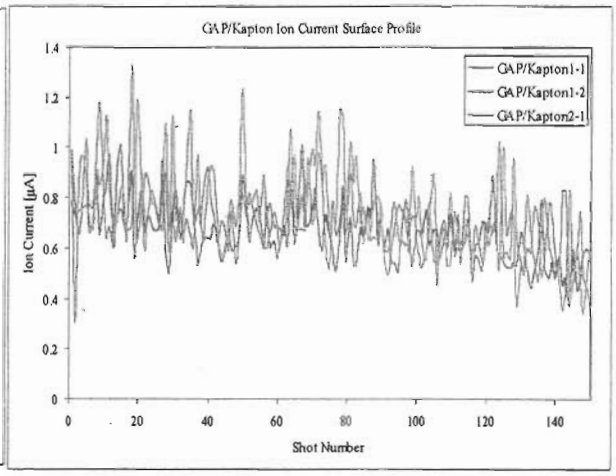

Figure 15. GAP/Kapton average ion currents. *The traces are for 24.5mJ deposited over 5ms. Traces were taken at 150 successive fuel locations. GAP/Kapton 1-1 represents one sample taken from fuel strip #1, whereas 2-1 and 2-2 indicate samples 1 and two taken from a separate fuel strip.*

PVC/Acetate

Of the two target materials, PVC and GAP, the PVC appears to exhibit more favorable performance characteristics. The PVC strip tested here was ~45μm thick with 115μm acetate backing (Figure 16a-16b). The thickness of the PVC is now half of the GAP/Kapton and reduced by a factor of 6 over the GAP/Acetate. Similar test conditions to the GAP were applied to the PVC testing where 24.5 mJ were deposited over 5 ms. However, the volume of mass ejected was $2.5 \times 10^{-7} cm^3$ corresponding to $3.4 \times 10^{-7} g$/shot or 0.34μg/shot of PVC ejected. The amount of PVC mass ejected is obviously much lower than either GAP case based on the reduced thickness of the PVC.

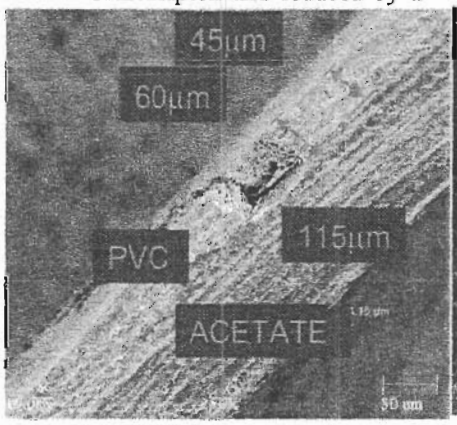

Figure 16a. PVC/Acetate SEM photo. *The cross-sectional view of the PVC/Acetate shows the thickness and depth of the ablation crater.*

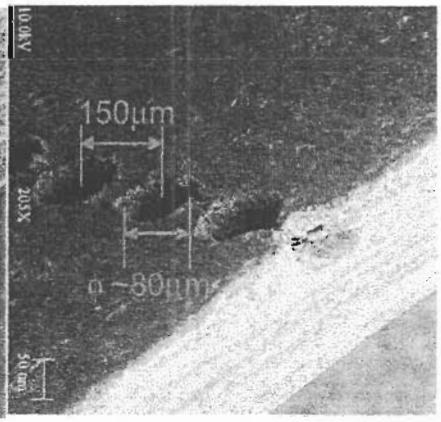

Figure 16b. PVC/Acetate SEM photo. *The distance between ablation events and across each crater is observed.*

Of the different fuel/substrate combinations, the PVC/Acetate had the highest average ion density of $7.9 \times 10^{9} cm^{-3}$ and an estimated ionization fraction of 5.1×10^{-7} at 6 cm from the target face. This was the downstream location where the greatest peak ion current was measured. In order to find this location, the ion current was measured at incremental distances downstream. This is illustrated in Figure 17.

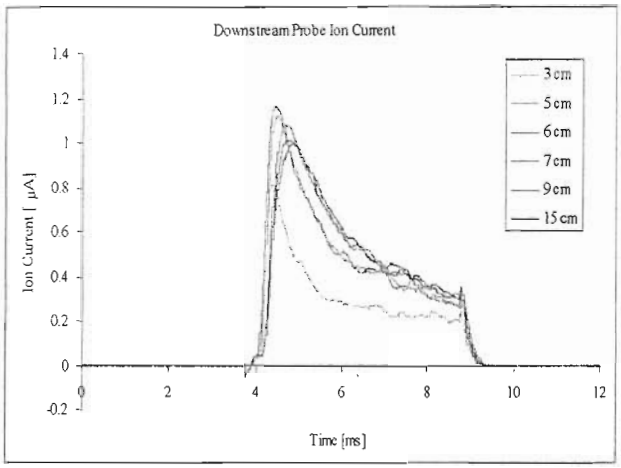

Figure 17. Downstream Probe Ion Currents. *The peak average ion current is seen to occur 6 cm downstream from the PVC face.*

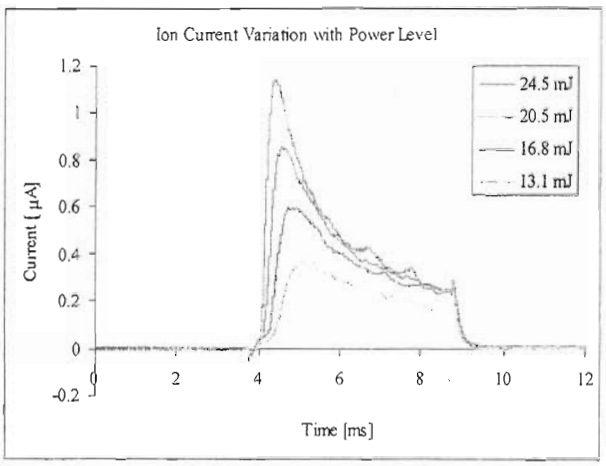

Figure 18. Ion current variation with increasing power. *With more energy deposited in the same time, the greater levels of ionization are achieved.*

Figure 17, this shows the current initially starts out small at 0.8 μA at 3 cm in front of the PVC and then rapidly expands to a peak value of 1.2 μA at 6 cm. This expansion is observed to take place within 100 μs.

In addition to seeing how the peak currents vary with downstream location, it is also of interest to see the effect of how the ion current changes by increasing the amount of deposited energy. Figure 18 shows the results of measuring the average ion current at increasing energy levels. The ion currents of the four measured energy levels are taken at 6 cm. This location was selected because it was found from Figure 17 to be the downstream location where the peak ion current occurs. By increasing the amount of energy deposited into the same amount of mass, Figure 18 illustrates how greater ion currents can be achieved as a result of increasing the kinetic temperature through greater incident energy.

A summary of the calculated results for each target material and substrate combination is shown in Table 2.

Table 2. Summary of Calculated Results for each Target/Substrate.

Fuel	Substrate	μg/shot	n_{ion} [cm^{-3}]	f [ionization fraction]
GAP	Acetate	5.1	1.6E+07	9.8E-09
GAP	Kapton	1.7	4.50E+07	8.20E-08
PVC	Acetate	0.34	7.90E+09	5.10E-07

V. Conclusion

Average ion currents and average ion densities have been measured on a μLPT using a negatively biased flat probe. These measurements were made for 24.5 mJ of energy deposited over a 5 ms discharge time for GAP and PVC materials. The results of these measurements show a very low ionization fraction in both PVC and GAP materials regardless of the substrate material that is backing them. One source of the low average ion currents and densities can be attributed to the relatively long discharge time of the μLPT. If this discharge time were to be shortened to the micro-second or nano-second length while maintaining the same amount of energy deposited to the target, a rise in the ionization levels should be expected. An additional method to increase the ionization level and in turn the I_{sp} of this propulsion device would be to optimize the fuel thickness. Measured ion currents indicate that a greater ionization is achieved in target materials that are incrementally thinner. This was evident as the peak ion current and the ionization fraction progressively increased from being low in the 300μm thick GAP to reaching the maximum for the 55μm thick PVC.

The peak ion currents measured at 150 successive locations over a 2.5 cm distance on a single fuel strip have also been measured. The results show how a material such as GAP, can have very different ion currents between transverse locations. This is an indication that a higher ion current implies a smaller thickness at the respective target

location. This would be because more laser energy is available for ionization rather than heating or neutral particle ejection.

Finally, the peak ion currents have been measured for PVC by increasing the amount of deposited laser energy. The more laser energy that is available for the same amount of PVC mass, results in a greater number of particles being ionized. This result is consistent with those observed in the GAP material that as the thickness of the material is reduced, greater levels of ionization are achieved. The SEM analysis confirms this result by showing equal ablation crater diameters for GAP when two different GAP thicknesses were considered. In both cases, the GAP ablation diameter was the same; however, the thicker GAP (300μm) resulted in a lower peak ion current and ionization fraction than the thinner GAP (115μm).

Acknowledgments

This work was funded by the Air Force Research Laboratory, Electric Propulsion Laboratory. We would like to thank Claude Phipps of Photonics Associates and Jim Luke of New Mexico Engineering Research Institute for providing the propulsion unit. Additionally, we would like to thank Wes Helgeson of Mew Mexico Engineering Research Institute for manufacturing multiple target/substrate combinations. Special thanks go to Marietta Hemdandez for providing spectacular images of the target and substrate materials from performing SEM measurements.

References

[1]Phipps, C.R., Luke, J.R., "Diode Laser-Driven Microthrusters: A new departure for micropropulsion," in *AIAA Journal,* Vol. 40 pp.310-318 (2002).

[2]Phipps, C.R., Luke, J.R., McDuff, G.G., and Lippert, T. "Laser Ablation Powered Mini-Thruster," in *High Power Laser Ablation IV*, edited by Claude R. Phipps, Editor, Proceedings of SPIE Vol. 4760 pp. 833-842 (2002).

[3]Jones, F.L., Willot, W.H., "Secondary emission from copper due to slow positive ions of argon," in Proceedings of the Physical Society, Vol. 48, pp. 830-838 (1936).

[4]Kubota, N., Aoki, I., "Burning Rate Characterization of GAP/HMX Energetic Composite Materials," in *Propellants, Explosives, Pyrotechnics,* Vol. 25 pp.168-171 (2000).

[5]"Material Safety Data Sheet; MSDS," URL: http://www.msds.com [cited 30 November 2001].

[6]Dupont, "Material Safety Data Sheet; MSDS," URL: http://www.dupont.com/kapton/index.html [cited 01 June 2005].

[7]Halliday, D., Resnick, R., Walker, J., *Fundamentals of Physics,* 7th ed., Wiley, 2004, Chaps. 21,22.

[8]Photonics,"Fiber Optics: Understanding the Basics," The *Photonics Design and Applications Handbook,* pp. H154-H157 (2002).